Lagrangian statistics in fully developed turbulence

L. BIFERALE*, G. BOFFETTA†# A. CELANI,‡, A. LANOTTE¶ and F. TOSCHI§

*Dipartimento di Fisica and INFN, Università degli Studi di Roma, "Tor Vergata", Via della Ricerca Scientifica 1, 00133 Roma, Italy
†Dipartimento di Fisica Generale and INFN, Università degli Studi di Torino, Via Pietro Giuria 1, 10125, Torino, Italy
‡CNRS, INLN, 1361 Route des Lucioles, 06560 Valbonne, France
¶CNR-ISAC, Sezione di Lecce, Str. Lecce-Monteroni km 1.2, 73100 Lecce, Italy
§Istituto per le Applicazioni del Calcolo, CNR, Viale del Policlinico 137, 00161 Roma, Italy

The statistics of Lagrangian particles transported by a three-dimensional fully developed turbulent flow is investigated by means of high-resolution direct numerical simulations. The analysis of single trajectories reveals the existence of strong trapping events vortices at the Kolmogorov scale which contaminates inertial range statistics up to $10\tau_\eta$. For larger time separations, we find that Lagrangian structure functions display intermittency in agreement with the prediction of the multifractal model of turbulence. The study of two-particle dispersion shows that the probability density function of pair separation is very close to the original prediction of Richardson of 1926. Nevertheless, moments of relative dispersion are strongly affected by finite Reynolds effects, thus limiting the possibility to measure numerical prefactors, such as the Richardson constant g. We show how, by using an exit time statistics, it is possible to have a precise estimation of g which is consistent with recent laboratory measurements.

1. Introduction

Understanding the Lagrangian statistics of advected tracers in fully developed turbulence is fundamental for developing stochastic models for dispersion and mixing in many physical applications [1–3]. Richardson's study on atmospheric dispersion [4] was the first experimental evidence of scaling law in fully developed turbulence. Despite the relevance of the problem, there are still relatively few data on turbulent Lagrangian statistics, if compared with Eulerian statistics. This is due to the intrinsic difficulty to experimentally measure Lagrangian trajectories in a fully developed turbulent flow. In order to obtain an accurate description of particle statistics, it is necessary to follow the trajectories for times comparable with the large-scale eddy turnover time T_L with a resolution of the order of the Kolmogorov time τ_η. The ratio of these timescales is estimated as $T_L/\tau_\eta \sim R_\lambda$, where the Taylor Reynolds number R_λ is of order of hundreds for typical laboratory experiments (and more in geophysical flows). Recent laboratory experiments were able to partially overcome these difficulties introducing new experimental techniques. By using a technique borrowed from high-energy physics, La Porta *et al.* [5] were able to obtain Lagrangian trajectories at very high resolution (of the order of one tenth of τ_η) in high R_λ turbulence. However, trajectories could be followed for few τ_η

#Corresponding author. E-mail: boffetta@to.infn.it

only. The acoustic Doppler technique developed by Mordant *et al.* [6] enabled them to obtain Lagrangian statistics for times comparable with T_L at a resolution of order of $5\tau_\eta$ but for a single velocity components and for a single particle. More conventional techniques, such as the stereographic particle tracking method adopted by Ott and Mann [7], are able to follow several trajectories simultaneously and for long time but only for small R_λ.

An alternative tool to investigate Lagrangian turbulence is represented by direct numerical simulations (DNS) where the complete Lagrangian statistics is resolved at the price of a moderate R_λ. In this contribution, we review recent results obtained from a set of DNS of Lagrangian transport in high-resolution homogeneous isotropic turbulence.

2. Direct numerical simulations of turbulence

Simulations were done on the IBM-SP4 parallel computer at Cineca on a cubic lattice at resolutions up to 1024^3 corresponding to $R_\lambda \simeq 280$. The Navier–Stokes equations for an incompressible ($\nabla \cdot \mathbf{u}$) flow

$$\partial_t \mathbf{u} + \mathbf{u} \cdot \nabla \mathbf{u} = -\nabla p + \nu \Delta \mathbf{u} + \mathbf{f} \qquad (1)$$

are integrated on a triply periodic cubic box by means of a fully dealiazed pseudospectral code with normal viscosity operator (see table 1 for numerical parameters). Energy is injected at the average rate ϵ by keeping constant the total energy in each of the first two wave number shells [8]. Starting from a zero-velocity initial condition, the system reaches a statistically stationary state for the velocity field with a well-developed spectral flux and Kolmogorov energy spectrum (see figure 1).

In stationary conditions, about two millions of Lagrangian tracers are injected into the flow and their trajectories integrated according to

$$\frac{d\mathbf{X}}{dt} = \mathbf{u}(\mathbf{X}(t), t), \qquad (2)$$

over a time lapse of the order of T_E (see animation 1, to which figure 2 refers). The Lagrangian velocity $\mathbf{v}(t) = \mathbf{u}(\mathbf{X}(t), t)$ was calculated using linear interpolation on the Eulerian grid. Particles' positions $\mathbf{X}(t)$ and velocities $\mathbf{v}(t)$ have been stored at a sampling rate $0.07\tau_\eta$. The forces acting on the particle—pressure gradients $\nabla p(\mathbf{X}(t), t)$, viscous forces $\nu \Delta \mathbf{u}(\mathbf{X}(t), t)$ and external forcing—and the resulting particle acceleration $\mathbf{a}(t) = \dot{\mathbf{v}}(t)$ (i.e. the rhs of (1)) have been recorded along the particle paths every $0.14\tau_\eta$.

The initial conditions of Lagrangian tracers are placed on the vertexes of small tetrahedrons at the Kolmogorov scale. This allows us to study the statistics of multiparticle dispersion and shape evolution [9]. In this contribution we will discuss the statistics of one-particle and two-particle dispersion.

Table 1.   Parameters of the numerical simulations. Microscale Reynolds number R_λ, root-mean-square velocity u_{rms}, energy dissipation ε, Kolmogorov lengthscale $\eta = (\nu^3/\varepsilon)^{1/4}$, large-eddy turnover time $T_E = L/u_{\mathrm{rms}}$, Kolmogorov timescale $\tau_\eta = (\nu/\varepsilon)^{1/2}$, total integration time T, box size L, grid spacing δx, resolution N and the number of Lagrangian tracers N_p.

R_λ	u_{rms}	ε	η	T_E	τ_η	T	L	δx	N	N_p
183	1.5	0.886	0.01	2.1	0.048	5	6.28	0.012	512	0.96×10^6
284	1.7	0.81	0.005	1.8	0.033	4.4	6.28	0.006	1024	1.92×10^6
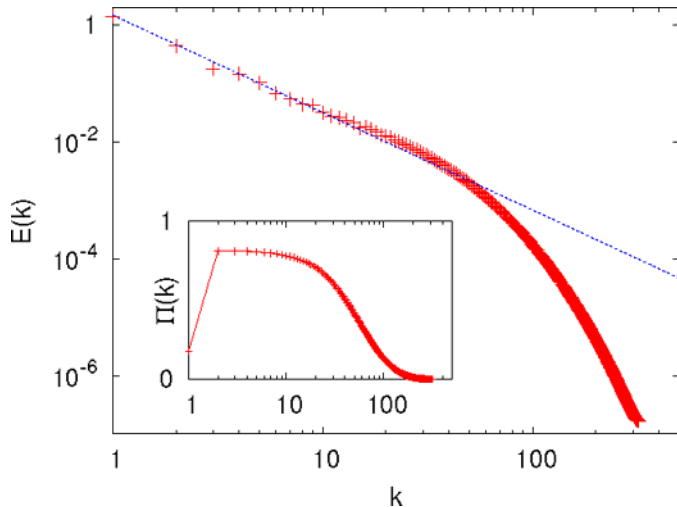
Figure 1. Energy spectrum and spectral flux (inset) for the $R_\lambda = 284$ simulation, averaged over one large-scale eddy turnover time. The line represents the Kolmogorov spectrum $E(k) = C\varepsilon^{2/3}k^{-5/3}$ with $C = 1.7$.

3. Single particle dispersion

A first characterization of Lagrangian dispersion is given by the autocorrelation function. This is defined from the Lagrangian velocities as

$$C^L(\tau) \equiv \frac{\langle \mathbf{v}(\tau) \cdot \mathbf{v}(0)\rangle}{\langle v^2 \rangle}, \tag{3}$$

where the average is taken over many trajectories. Figure 3 shows that the decrease of the autocorrelation is well approximated by an exponential function $C^L(\tau) \simeq \exp(-\tau/T_L)$ which defines the Lagrangian integral characteristic time $T_L \simeq 1.3$. The deviations of $C^L(\tau)$ from the exponential function shown in figure 3 are a consequence of the fluctuation of large-scale quantities (such as the total energy) in our single run simulation. We have checked that
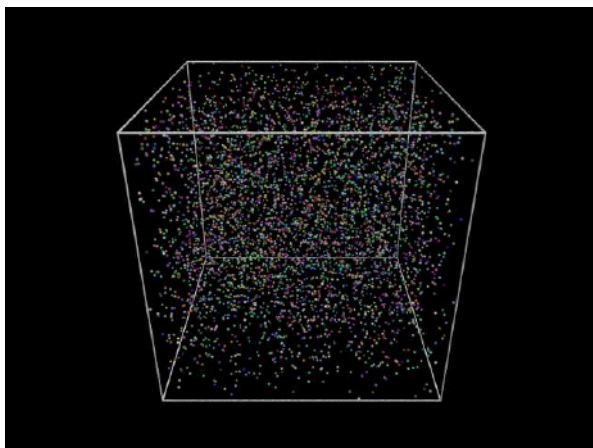
Figure 2. Time evolution of 4800 Lagrangian tracers in the turbulent flow at $R_\lambda = 284$ (animation 1, size 5.7 Mbyte, format MPEG-1).
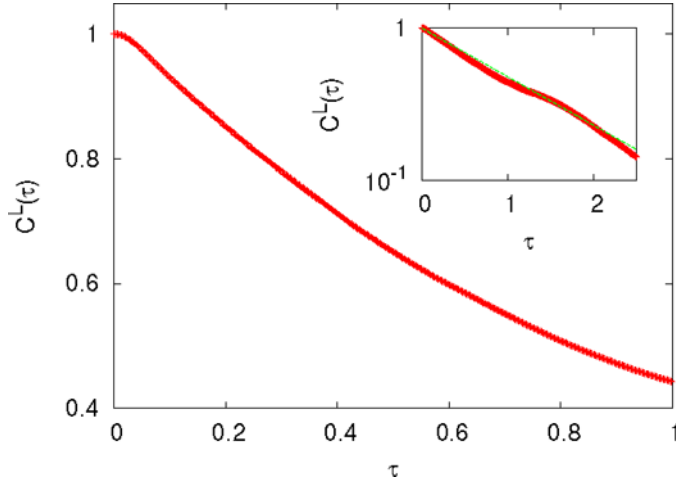
Figure 3.   Lagrangian velocity autocorrelation function in linear coordinates and lin-log (inset) for the $R_\lambda = 284$ run. For comparison the exponential fit $\exp(-\tau/T_L)$ is also shown.

large-scale fluctuations do not affect small-scale statistics which evolve on much faster time scales.

The exponential decay of the autocorrelation function is a fundamental result as it is at the basis of the stochastic models of turbulent dispersion [2]. Nevertheless, the analysis of single Lagrangian trajectories reveals that turbulent dispersion is much more complex than random dispersion. Figure 4 shows the trajectory of a particle which remains trapped within a vortical structure for a rather long time. By numerically tracking velocity and acceleration of single particles, one recognizes that these trapping events are at the origin of extreme fluctuations in velocity and acceleration statistics (as shown in the insets of figure 4), which are not described by simple stochastic processes. The analysis of our simulations reveals that these events are not infrequent and dominate the tails of probability density functions (pdf) of velocity fluctuations and acceleration.
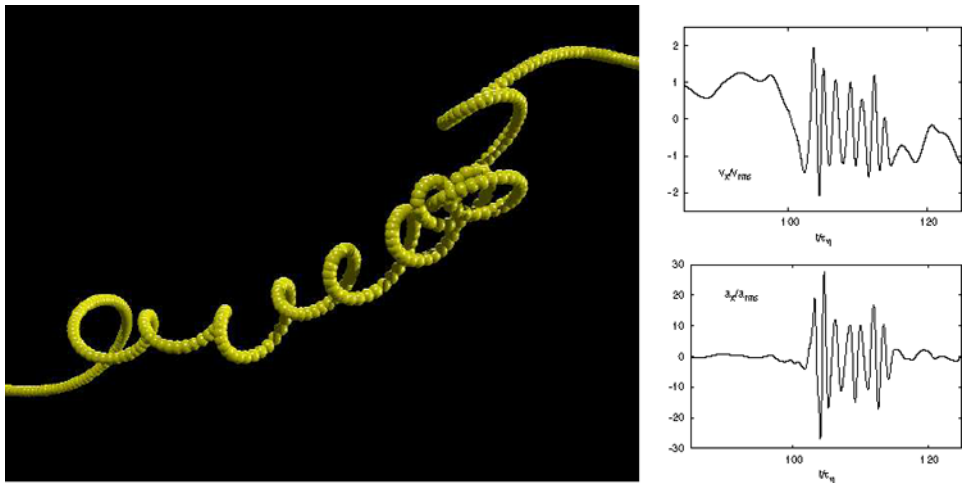
Figure 4.   Trajectory and time series. *Left panel*: Three-dimensional trajectory of a trapping event in a vortex filament. The sampling time is $\Delta t = 0.07\tau_\eta$ and $R_\lambda = 284$. Acceleration and velocity fluctuations for this event reach values as large as 30 and 2 rms, respectively (see right-hand panels).
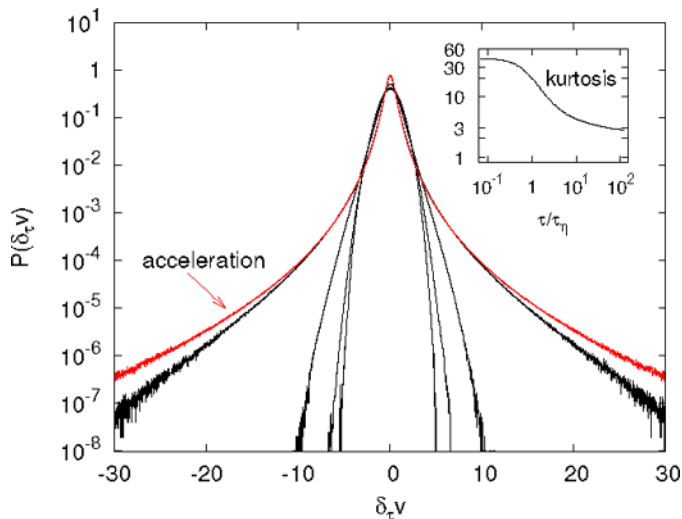
Figure 5. Probability density functions of velocity increments and acceleration for the $R_\lambda = 284$ run. Curves refer to time increments $\tau = (97, 24, 6, 0.7)\tau_\eta$ from inside to outside and to the acceleration. In the inset flatness $F(\tau) = \langle \delta_\tau v^4 \rangle / (\langle \delta_\tau v \rangle^2)^2$ for the entire time interval $(0.07\tau_\eta, 2T_E)$. The saturation of $F(\tau)$ at small time increments is an indication of the high-numerical resolution.

Figure 5 shows the pdf of Lagrangian acceleration. In agreement to what was observed in laboratory experiments at higher R_λ [5], the pdf is characterized by large stretched exponential tails with flatness $F \simeq 40$, comparable to the experimental value obtained at a similar R_λ. The form of the acceleration pdf has recently been the object of intense research based on different physical models. Of course, the form of the acceleration pdf cannot be universal as it is, at least, parameterized by R_λ. In [10], the present authors have shown how the multifractal model of turbulence [11] can be used to predict the acceleration pdf without additional free parameters.

Figure 5 also shows the pdfs of Lagrangian velocity increments $\delta_\tau v = v(\tau) - v(0)$ at different values of time lag τ from $\tau \simeq \tau_\eta$ to $\tau \simeq 100\tau_\eta$. By increasing the time separation, the pdfs become decreasingly intermittent and eventually saturate to a distribution very close to Gaussian for $\tau \simeq T_L$, as indicated by the flatness shown in the inset. Also in this case, the form of the numerically obtained pdfs shown in figure 5 is in qualitative agreement with experimental results [6].

The intermittency of Lagrangian time increments δ_τ observed in the pdf can be conveniently quantified in terms of the scaling exponents ξ_p of the Lagrangian structure functions

$$S_p^{(L)}(\tau) \equiv \langle (\delta_\tau v)^p \rangle \simeq \tau^{\xi_p}. \tag{4}$$

Dimensional analysis [1] predicts for the second-order structure function a linear scaling in τ, $S_2^{(L)}(\tau) = C_0 \varepsilon \tau$ (i.e. $\xi_2 = 1$), with a universal dimensionless constant C_0. There is still no clear evidence of the linear scaling for the second-order structure function, even in the case of high Reynolds number experiments [6], and as a consequence the value of C_0 is still largely uncertain [12]. In the following, we will propose an interpretation of this poor scaling in terms of trapped trajectories such the one shown in figure 4.

Because Lagrangian velocity increments are intermittent, we cannot expect for the higher order structure functions the dimensional scaling $\xi_p = p/2$. It is possible to give a prediction of the Lagrangian scaling exponents in terms of the multifractal model of turbulence. The typical velocity fluctuation on a time lag τ is given by $\delta_\tau v \simeq \delta_\ell v$, where ℓ is the scale of eddies with characteristic time $\tau(\ell) \simeq \tau$. Using that $\delta_\ell v \sim \ell^h$ with probability $P(h) \sim \ell^{3-D(h)}$ and that

$\tau(\ell) \sim \ell^{1-h}$ [11], one ends with the prediction [13]:

$$\xi_p = \min_h \left[\frac{ph + 3 - D(h)}{1 - h} \right].$$ (5)

The fractal dimension $D(h)$ is expressed in terms of Eulerian velocity structure functions, and it is thus given (from Eulerian experimental data or from phenomenological models). The standard inequality in the multifractal model (following from the Kolmogorov 4/5-law) $D(h) \leq 3h + 2$ implies for (5) that $\xi_2 = 1$ even in the presence of intermittency (this is a consequence of the fact that in the second-order Lagrangian structure function, the energy dissipation ε appears with the first power). For a comparison with our numerical data, in the following, we will use for $D(h)$ an empirical formula which fits very well the experimental data [14].

The behaviour of the first $S_p^{(L)}(\tau)$ from our simulations is shown in figure 6 [15] for the three components. Structure functions on different components deviate at large delays, as a consequence of a certain degree of anisotropy at large-scales. This effect could be removed only after averaging over many large-scale eddy turnover times. As it is evident from the inset of figure 6, it is very difficult to extract the values of ξ_p from the logarithmic slope, in particular for higher p. We thus decided to assume the scaling for the second-order structure function $\xi_2 = 1$ and to compute *relative* scaling ξ_p/ξ_2 by using the so-called extended self-similarity procedure [16]. As shown by the inset of figure 6, we observe a well-defined scaling in the range of separations $10\tau_\eta \leq \tau \leq 50\tau_\eta$. The values of the relative exponents estimated with this method, $\xi_4/\xi_2 = 1.7 \pm 0.05$, $\xi_5/\xi_2 = 2.0 \pm 0.05$, $\xi_6/\xi_2 = 2.2 \pm 0.07$, are in good agreement
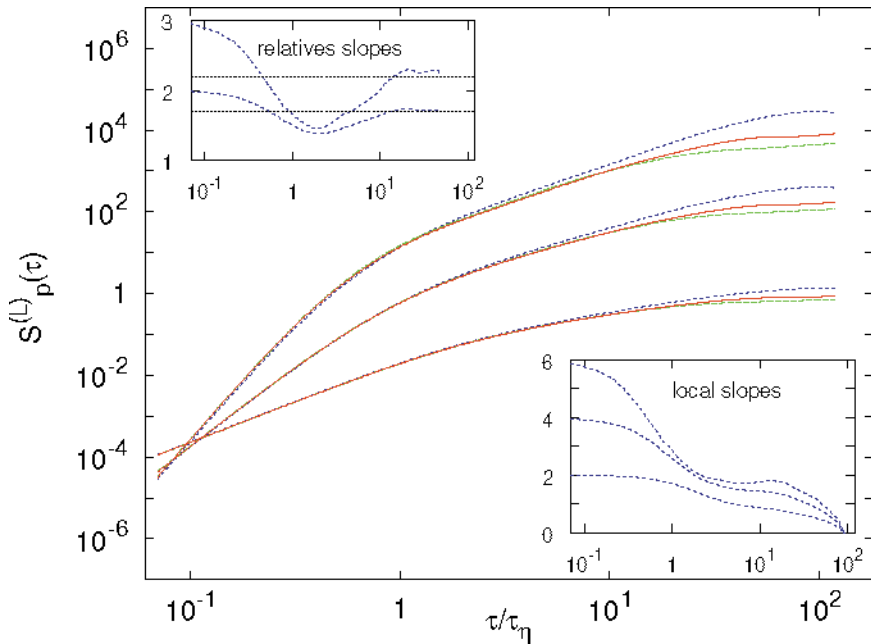
Figure 6. Log-log plot of Lagrangian structure functions of orders $p = 2, 4, 6$ (bottom to top) versus τ, along the three spatial directions. At any order p, from top to bottom we have the x, z, y components, respectively. In the inset on the bottom right, logarithmic local slopes of all orders are shown for the x-component, the most energetic one. In the inset on the top-left, relative local slopes, with respect to the second order, are shown d log $S_p(\tau)$/d log $S_2(\tau)$ for $p = 4, 6$ and the x-component, together with the multifractal predictions (line). Data refer to $R_\lambda = 284$.

with those predicted by the multifractal model (5) and with the experimental values obtained in [6].

It is interesting to observe that at small time lag τ, from τ_η to $10\tau_\eta$, local slopes of all orders tend to accumulate around the value 2. A possible interpretation of these strong deviations in the scaling laws is in terms of entrapment events of Lagrangian trajectories within vortical structures, as in the example of figure 4. The Lagrangian velocity in this case displays fluctuations up to $5u_{\mathrm{rms}}$ on a time scale τ_η, while the duration of the event can be as long as $10\tau_\eta$. Thus for $\tau_\eta \le \tau \le 10\tau_\eta$ trapped particle see velocity fluctuations almost discontinuous (i.e. $h = 0$) on a one-dimensional structure (i.e. $D(h) = 1$). Inserting these values in (5) one has the prediction $\xi_p = 2$ for any p which is consistent to what is observed in figure 6.

4. Two-particle dispersion

Relative dispersion of two particles is historically the first issue quantitatively addressed in the study of fully developed turbulence. This was done by Richardson, in a pioneering work on the properties of dispersion in the atmosphere in 1926 [4], and then reconsidered by Batchelor [17], among others, in the light of Kolmogorov 1941 theory [11].

Richardson's description of relative dispersion is based on a diffusion equation for the probability density function $p(\mathbf{r}, t)$, where $\mathbf{r}(t) = \mathbf{X}_2(t) - \mathbf{X}_1(t)$ is the separation of two trajectories generated by (2). In the isotropic case, the diffusion equation can be written as

$$\frac{\partial p(\mathbf{r}, t)}{\partial t} = \frac{1}{r^2} \frac{\partial}{\partial r} r^2 K(r) \frac{\partial p(\mathbf{r}, t)}{\partial r},$$ (6)

where the turbulent eddy diffusivity was empirically established by Richardson to follow the 'four-thirds law': $K(r) = k_0 \varepsilon^{1/3} r^{4/3}$. The scale dependence of diffusivity is at the origin of the accelerated nature of turbulent dispersion: particle relative velocity grows with the separation (see figure 7 for animation 2). Richardson's empirical formula is a simple consequence of Kolmogorov scaling in turbulence, as first recognized by Obukhov [23].
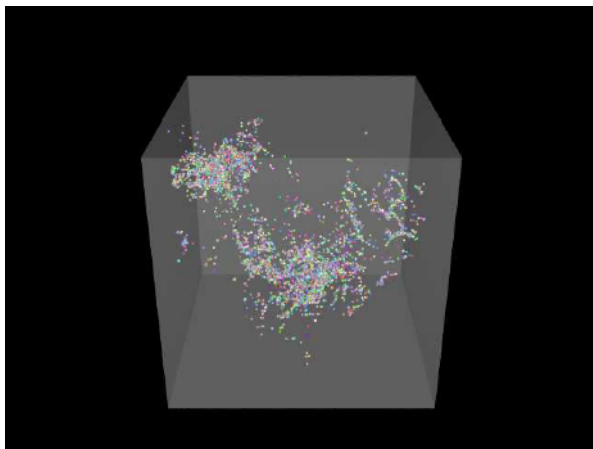
Figure 7. Evolution of a cluster of 8192 Lagrangian particles in a turbulent flow at $R_\lambda = 284$ (animation 2, size 4.4 Mbyte, format MPEG-1).
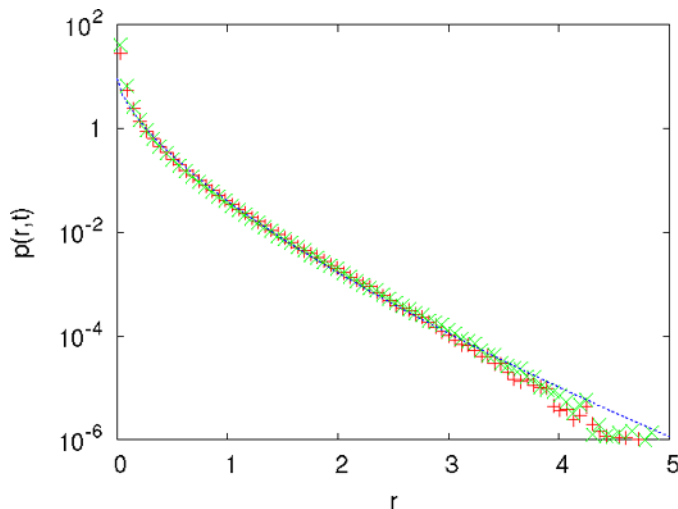
Figure 8.   Probability density functions of particle separations normalized with their variance at two different times $t = 0.2T_L$ (red) and $t = 0.4T_L$ (green). Initial particle separation $r_0 = \delta x$, $R_\lambda = 284$. The blue line represents the Richardson distribution (7).

The solution of (6) for δ-distributed initial condition has the well-known stretched exponential form

$$p(\mathbf{r}, t) = \frac{A}{(k_0 \varepsilon^{1/3} t)^{9/2}} \exp\left(-\frac{9r^{2/3}}{4k_0 \varepsilon^{1/3} t}\right) \tag{7}$$

where A is a dimensionless normalizing factor. There are presently not so many numerical [18–21], and very few laboratory experimental [7, 22] studies on relative dispersion in turbulence. As a consequence, there is still no general consensus on the form of the pdf of two-particle dispersion in turbulence. The first experimental data were obtained in geophysical contexts (see [1] and [24] for a review) and were not able to confirm the stretched exponential form (7). Recent laboratory experiments showed that in homogeneous isotropic turbulence the Richardson model is consistent with the measurements [7].

Figure 8 shows the pdfs of pair separation normalized with their variance at two different times. For intermediate times, which correspond to mean separations within the inertial range, we observe a collapse of the $p(\mathbf{r}, t)$ which justifies the hypothesis of self-similarity, implicit in (6). Moreover, the agreement with the Richardson distribution is remarkable. Some deviations from (7) are observable as large separations ($r \geq 4r_{\mathrm{rms}}$) where the statistics is affected by finite-size effects.

The complete determination of the statistics of pair separation requires the measure of a dimensionless coefficient, such as k_0 in (6). Traditionally, previous investigations have concentrated on the so-called Richardson constant g which enters the law for the evolution of the variance

$$\langle r^2(t) \rangle = g \varepsilon t^3. \tag{8}$$

The value of g is still known with a large uncertainty. Recent experimental [7] and numerical [20] investigations suggest a value $g \simeq 0.5$, but at moderate values of R_λ. Figure 9 shows that even at the present resolution, the behaviour of $\langle r^2(t) \rangle$ at intermediate times (corresponding to separations within the inertial range) still feels the initial separation r_0. This makes the direct determination of g very difficult, as shown in the inset of figure 9.
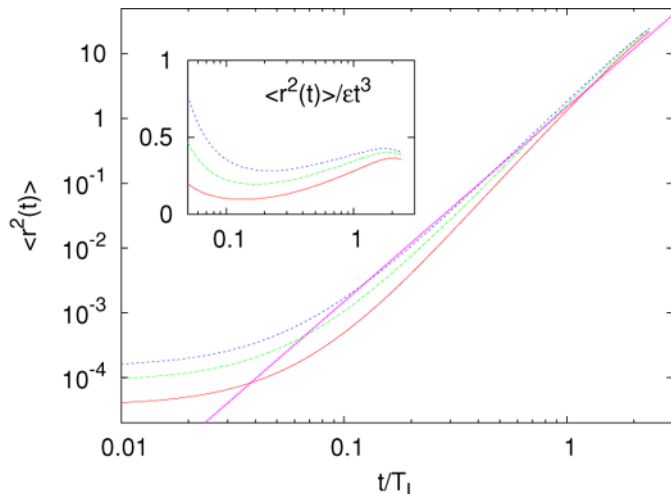
Figure 9. Variance of relative dispersion versus time for three different initial separations $r_0 = (1, 1.54, 2)\delta x$ (bottom to top). The line is the power law (8). Inset: compensated plot $\langle r^2(t)\rangle/\varepsilon t^3$ for the three separations (same colours).

An alternative approach for Lagrangian statistics is based on exit time statistics [25]. The idea behind this method is to compute the doubling time $T_\rho(R)$ which takes for the separation to grow from R to ρR (with $\rho > 1$). This is a first passage problem for the diffusion equation (6) which can be solved to give (see Appendix)

$$\langle T_\rho(R)\rangle = \frac{\rho^{2/3} - 1}{2k_0 \varepsilon^{1/3} \rho^{2/3}} R^{2/3}. \tag{9}$$

The outstanding advantage of averaging at fixed-scale separations, as opposite to fixed time, is that it removes crossover effects since all the sampled separations belongs to the same scale. Figure 10 shows the mean exit time for the two runs at different R_λ. The improvement of the
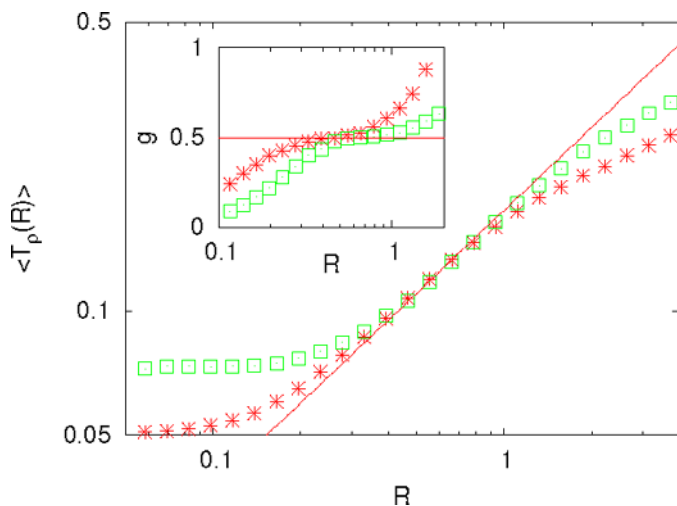
Figure 10. Mean doubling time of pair separation $\langle T_\rho(R)\rangle$ with $\rho = 1.19$ at resolutions $N = 512$ ($\square$) and $N = 1024$ ($*$). The line represent the dimensional scaling $R^{2/3}$.
Inset: compensated plot $143(\rho^{2/3} - 1)^3 R^2/(81\rho^2\varepsilon\langle T_\rho\rangle^3)$ which gives the Richardson constant g.
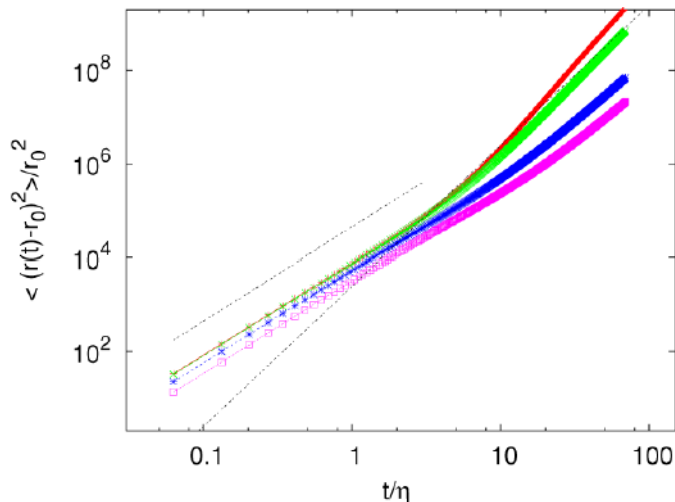
Figure 11.   Time evolution of the mean-square particle separation $\langle[\mathbf{r}(t) - \mathbf{r_0}]^2\rangle$, for the run with $R_\lambda = 284$. Curves refer to four different initial separations $r_0 = (1, 2, 8, 16)\,\delta x$ from top to the bottom, respectively. Each curve has been scaled with r_0^2. The two lines represent the scaling t^2 and t^3.

scaling with respect to figure 9 is evident. In the inset, $\langle T_\rho(R)\rangle$ is compensated according to (9) to give the value of $g \simeq 0.5$.

Before ending this section, we would like to comment on the short-time behaviour of the mean-square distance of particles' pairs $\langle r^2(t)\rangle$. According to Batchelor [17], before the Richardson's behaviour (8) sets in, there is a time range for which particles continue to move with their initial velocities $u(\mathbf{X}_1(0), 0)$, $u(\mathbf{X}_2(0), 0)$, and do not change the underlying velocity fluctuation. To be more precise, the provided initial separation r_0 is much smaller than the integral scale of the motion L, pair separation should behave as

$$\langle[\mathbf{r}(t) - \mathbf{r_0}]^2\rangle \sim \left[S_2^E(\mathbf{r_0})\right]t^2 \quad t < t^*, \tag{10}$$

while for times $t \gg t^*$ it should recover the Richardson law (9), where the dependency from initial separation is no longer present. In the previous expression, the Eulerian second-order structure function $S_2^E(R) \equiv \langle[u(\mathbf{x_0}+\mathbf{R})-u(\mathbf{x_0})]^2\rangle$ is measured at the initial relative distance r_0, and it clearly varies for r_0 belonging to the Eulerian dissipative or inertial range. Observations of Batchelor's behaviour have recently been reported in experiments [22].

In figure 11, we show the time behaviour of the relative dispersion $\langle[\mathbf{r}(t) - \mathbf{r_0}]^2\rangle$ for particles' pairs with four different initial separations $r_0 = (1, 2, 8, 16)\delta_x$, and for $R_\lambda = 284$. It is useful to recall that in our run the Eulerian dissipative scales are well resolved, satisfying the condition $\eta \sim \delta x$, where δx is the grid spacing, so that at least initial separations of the order of $r_0 = (1, 2)\delta_x$ lie in the dissipative range. The collapse observed at short times for the two smallest separations indicates that pair separation effectively grows as $\langle[\mathbf{r}(t) - \mathbf{r_0}]^2\rangle \sim C_1(\varepsilon r_0^2)t^2$. Contrarily, as the initial separations $r_0 = (8, 16)\,\delta x$ are at the edge of the dissipative range, the related curves do not exactly collapse onto the others.

It can be noticed that for $r_0 = (1, 2)\delta_x$ the t^2 behaviour holds for a time t^* of the order of few τ_η. Such time slowly increases with the initial separation r_0, in agreement with the fact that in this regime, due to the exponential growth of particles' separation, we should have $t^* \sim \log(r_0)$. For initial separations $r_0 = (8, 16)\,\delta x$ the time t^* also grows with the initial separation, but with a rate $\propto r_0^{2/3}$. Finally, for larger times all curves deviate from Batchelor's t^2 evolution (10), and tend to recover Richardson behaviour, whose direct observation, as

previously remarked, is made difficult because of the contamination of the inertial range due to the dissipative and integral scales. We remark again that this kind of finite-size effects disappears when using the exit time statistics, as it is evident from figure 10.

5.   Conclusions

In this contribution, we have reviewed recent developments in turbulent Lagrangian dispersion achieved by means of high-resolution DNS. The advantage of DNS, with respect to present laboratory experiments, is the possibility to obtain reliable statistics in a large range of separations, from the Kolmogorov to the integral time scale for many simultaneous trajectories. The price to pay is a moderate Reynolds number which limits the extension of the inertial range. We have shown that this limitation can be overcome by implementing alternative analysis tools, such as extended self-similarity and exit time statistics.

Acknowledgments

Appendix

Mean doubling time is obtained from a stationary solution of the Richardson diffusion equation (6). Imagine that one particle per unit time is introduced at $r = R/\rho$, and there are, respectively, reflecting and absorbing boundaries at $r = 0$ and $r = R$. The stationary solution in three dimensions is

$$p(r) = \begin{cases} C[\rho^{7/3} - 1] & \text{for } 0 < r < R/\rho \\ C\left[\left(\dfrac{r}{R}\right)^{-7/3} - 1\right] & \text{for } R/\rho < r < R. \end{cases} \tag{A.1}$$

The number of particle in $r < R$ is

$$N = \int_{|\mathbf{r}|<R} p(r)\mathrm{d}\mathbf{r} = 4\pi \int_0^R r^2 p(r)\mathrm{d}r \tag{A.2}$$

By using (A.1), one obtains

$$N = (14\pi/3)C(1 - \rho^{-2/3})R^3. \tag{A.3}$$

The current at $r = R$, i.e. the number of particle exiting from the boundary R per unit time, is given by

$$J = -\frac{\mathrm{d}}{\mathrm{d}t} \int_{|\mathbf{r}|<R} p(r)\mathrm{d}\mathbf{r} = (28\pi/3)C\varepsilon^{1/3}k_0 R^{7/3}. \tag{A.4}$$

The mean doubling time is the average time spent by a particle at $r < R$. It is given by the ratio N/J and thus

$$\langle T_\rho(R) \rangle = \frac{\rho^{2/3} - 1}{2\varepsilon^{1/3}k_0\rho^{2/3}} R^{2/3} \tag{A.5}$$

which is (9).

References

[1]   Monin, A.S. and Yaglom, A.M., 1975, *Statistical Fluid Mechanics* (MIT Press, Cambridge, MA).
[2]   Pope, S.B., 2000, *Turbulent Flows* (Cambridge University Press, Cambridge).
[3]   Yeung, P.K., 2002, *Annu. Rev. Fluid Mech.* **34**, 115.
[4]   Richardson, L.F., 1926, *Proc. Roy. Soc.* A **110**, 709.
[5]   La Porta, A., Voth, G.A., Crawford, A.M., Alexander, J. and Bodenschatz, E., 2001, *Nature*, **409**, 1017.
[6]   Mordant, N., Metz, P., Michel, O. and Pinton, J.F., 2001, *Phys. Rev. Lett.*, **87**, 214501.
[7]   Ott, S. and Mann, J., 2000, *J. Fluid Mech.*, **422**, 207.
[8]   Chen, S., Doolen, G.D., Kraichnan, R.H. and She, Z.S., 1993, *Phys. Fluids*, A **5**, 458.
[9]   Pumir, A., Shraiman, B.I. and Chertkov, M., 2000, *Phys. Rev. Lett.*, **85**, 5324.
[10] Biferale, L., Boffetta, G., Celani, A., Devenish, B.J., Lanotte, A. and Toschi, F., 2004, *Phys. Rev. Lett.*, **93**, 064502.
[11] Frisch, U., 1995, *Turbulence* (Cambridge University Press, Cambridge).
[12] Lien, R.C. and D'Asaro, E.A., 2002, *Phys. Fluids*, **14**, 4456.
[13] Boffetta, G., De Lillo, F. and Musacchio, S., 2002, *Phys. Rev.*, E **66**, 066307.
[14] She, Z.S. and Leveque, E., 1994, *Phys. Rev. Lett.*, **72**, 336.
[15] Biferale, L., Boffetta, G., Celani, A., Lanotte, A. and Toschi, F., 2005, *Phys. Fluids*, **17**, 021701.
[16] Benzi, R., Ciliberto, S., Tripiccione, R., Baudet, C., Massaioli, F. and Succi, S., 1993, *Phys. Rev.*, E **48** R29
[17] Batchelor, G.K., 1950, *Q. J. R. Meteorol. Soc.*, **76**, 133.
[18] Yeung, P.K., 1994, *Phys. Fluids*, **6**, 3641.
[19] Ishihara, T. and Kaneda, Y., 2002, *Phys. Fluids*, **14**, L69.
[20] Boffetta, G. and Sokolov, I.M., 2002, *Phys. Rev. Lett.*, **88**, 094501.
[21] Yeung, P.K. and Borgas, M.S., 2004, *J. Fluid Mech.*, **503**, 93.
[22] Bourgoin, M., Ouellette, N.T., Xu, H., Joergensen, J.B. and Bodenschatz, E., 2005, preprint available at http://xxx.lanl.gov, *e-print ArXiv* physics/0503169.
[23] Obukhov, A.M., 1941, *Izv. Akad. Nauk. SSSR*, **5**, 453.
[24] Sawford, B., 2001, *Annu. Rev. Fluid Mech.*, **33**, 289.
[25] Artale, V., Boffetta, G., Celani, A., Cencini, M. and Vulpiani, A. 1997, *Phys. Fluids*, A **9**, 3162.